The Impact of Excess Lead Iodide on the Recombination Kinetics in Metal Halide Perovskites

Aboma Merdasa,[1,] Alexander Kiligaridis,[2] Carolin Rehermann,[1] Mojtaba Abdi-Jalebi,[3] Jonas Stöber,[2] Boris Louis,[2] Marina Gerhard,[2] Samuel D. Stranks,[3] Eva L. Unger,[1,2,*] and Ivan G. Scheblykin[2,*]*

[1]Young Investigator Group Hybrid Materials Formation and Scaling, Helmholtz-Zentrum Berlin für Materialen un Energie GmbH, Albert-Einstein Strasse 16, 12489 Berlin, Germany.
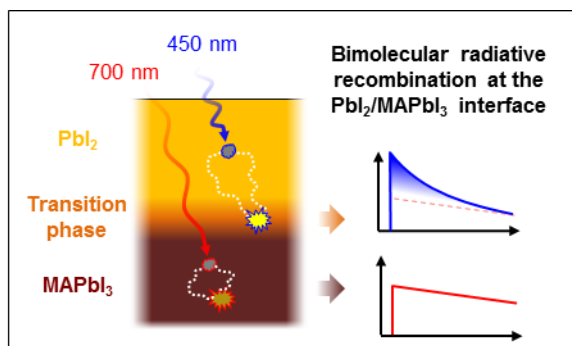
[2]Chemical Physics and NanoLund, Lund University, PO Box 118, 22100 Lund, Sweden.

[3]Cavendish Laboratory, Department of Physics, University of Cambridge, JJ Thomson Avenue, Cambridge CB3 0HE, United Kingdom.

Abstract

Fundmental comprehension of light-induced processes of perovskites are still scarce. One active debate surrounds the influence of excess lead iodide (PbI_2) on device performance, as well as optoelectronic properties, where both beneficial and detrimental traits have been reported. Here, we study its impact on the charge-carrier recombination kinetics by simultaneously acquiring photoluminescence quantum yield and time-resolved photoluminescence as a function of excitation wavelength (450 nm - 780 nm). The presence of PbI_2 in the perovskite film is identified via a unique spectroscopic signature in the PLQY spectrum. Probing the recombination in the presence and absence of this signature, we detect a radiative bimolecular recombination mechanism induced by PbI_2. Spatially resolving the photoluminescence, we determine that this radiative process occurs in a small volume at the PbI_2/perovskite interface, which is only active when charge carriers are generated in PbI_2, and therefore provide deeper insight into how excess PbI_2 may improve the properties of perovskite based devices.

TOC GRAPHICS

Metal halide perovskites have in merely a decade become strong contenders for absorber materials in commercially competitive solar cells, where recent advances are yielding power conversion efficiencies approaching that of silicon based devices.[1–3] One limiting factor has long been the issue of poor stability under operational conditions, which for some time seemed an unfeasible hurdle to overcome. However, recent progress in compositional engineering of metal-halide perovskite absorbers demonstrates that this is becoming less of an obstacle,[4,5] resulting in improved efficiency and stability under concentrated illumination.[6] Investigating the effect of long-term light exposure is of crucial importance to predict the intrinsic material stability and design more stable alternatives.

It is known that lead-iodide based metal halide perovskite semiconductors decompose into lead iodide (PbI_2) when exposed to a range of external stimuli, of which photons are highly relevant.[7–14] While decomposition of the perovskite absorber is clearly an undesirable effect, reports emerged early hinting toward beneficial aspects with excess PbI_2.[15–17] This sparked a debate around the role residual PbI_2 actually plays, generating a number of publications dealing with the impact on material[18–20] and device properties,[21–23] which is nicely summarized by Jacobsson and co-workers.[24] Today, the general consensus seems to be that a slight excess of PbI_2 improves key device parameters such as the open-circuit voltage (V_{OC}), short-circuit current (J_{SC}), and power conversion efficiencies (η), but at the cost of reduced long-term stability.[25,26]

From a more fundamental perspective, it has been demonstrated that recombination between charge carriers in the absorber and transport layers have been suppressed due to a thin interfacial layer of PbI_2.[27–29] In regard to charge carriers that form in the perovskite absorber, both a reduction of non-radiative recombination, and accelerated recombination with an excess of PbI_2 has been reported.[30–32] These reports do not necessarily contradict one another but may rather

3

reflect a dependence on where, and how PbI_2 has been introduced in the perovskite. So far, investigations have focused on charge carriers formed in the $MAPbI_3$ layer only, while those that form in PbI_2 are assumed parasitically lost and therefore not considered to partake in subsequent recombination mechanisms.

Recombination of charge carriers is an important factor dictating the performance of a solar cell device, where non-radiative recombination should ideally be eliminated.[33] This aspect is of key relevance when examining the properties of the absorber material without transport layers or contacts. Photoluminescence quantum yield (PLQY) measurements become important as they provide a qualitative measure of the competition between radiative and non-radiative processes. While both steady-state and time-resolved photoluminescence (PL) experiments are used as standard methods to characterize the optoelectronic properties of perovskite absorbers, as well as predict device performance,[34–36] a few considerations must be made. Steady-state PL alone cannot provide information on the recombination dynamics of photo-generated charge carriers and should hence be complemented with time-resolved PL (TRPL) measurements. At the same time, a long carrier lifetime can be obtained even if the PLQY is low, which may therefore by itself be a misleading figure of merit when assessing potential device performance, unless accompanied with extensive modeling.[37] Thus, in order to better characterize the light conversion properties of a material, and also describe the underlying recombination processes via optical probes, TRPL and PLQY should be, where possible, performed in a complementary manner.[38]

Herein, we present a study on the recombination kinetics in methylammonium lead triiodide ($MAPbI_3$) films and the impact caused by PbI_2 when introduced as a photo-induced degradation product over several hours, as well as via vapour-assisted deposition. Extracting the PLQY as a function of wavelength (450 nm – 780 nm) during light-soaking we find a unique spectral

signature related to PbI_2 allowing us monitor its formation in time. By simultaneously acquiring the time-resolved PL at excitation wavelengths between 450 nm – 700 nm, we identify a change the in charge carrier recombination mechanism occurring in $MAPbI_3$ facilitated by PbI_2. Employing fluence dependent TRPL and spatially resolved spectroscopic measurements, we determine that charge carriers generated in PbI_2 funnel to a transition phase interlinking PbI_2 and $MAPbI_3$ where they undergo radiative bimolecular recombination with a blue-shifted PL emission in relation to typical $MAPbI_3$ emission (775 nm). Our observations therefore provide necessary insight into how the overall recombination kinetics in $MAPbI_3$ may be altered by PbI_2, which may further resolve some of the ambiguity surrounding the role of PbI_2 in regard to both material and device properties.

Spectrally Resolved PL Quantum Yield

   $MAPbI_3$ thin films were prepared inside a glove box on thin glass substrates according to the methods outlined in the Supporting Information, where structure and morphology of the films were characterized by SEM and XRD (see SI Note 1). Optical characterization was made in a novel microscope developed to simultaneously measure PL excitation spectra together with absorptance in the wavelength range of 450 nm – 780 nm. For excitation, we employed a tunable pulsed laser source, allowing us to also acquire the time-resolved PL (see SI for further details). PLE spectra were acquired by scanning the excitation from 450 nm to 780 nm while integrating PL from the tail of the emission band above 790 nm (Figure 1a). Calibrating the excitation density to 0.1 W/cm^2 (1 Sun), we simultaneously light-soak the sample while also probing the optoelectronic properties (see SI Note 2 for details). Unless otherwise noted, measurements were

conducted such that the excitation impinges on the material side of the sample, where PL also is collected (see inset in Figure 1a).
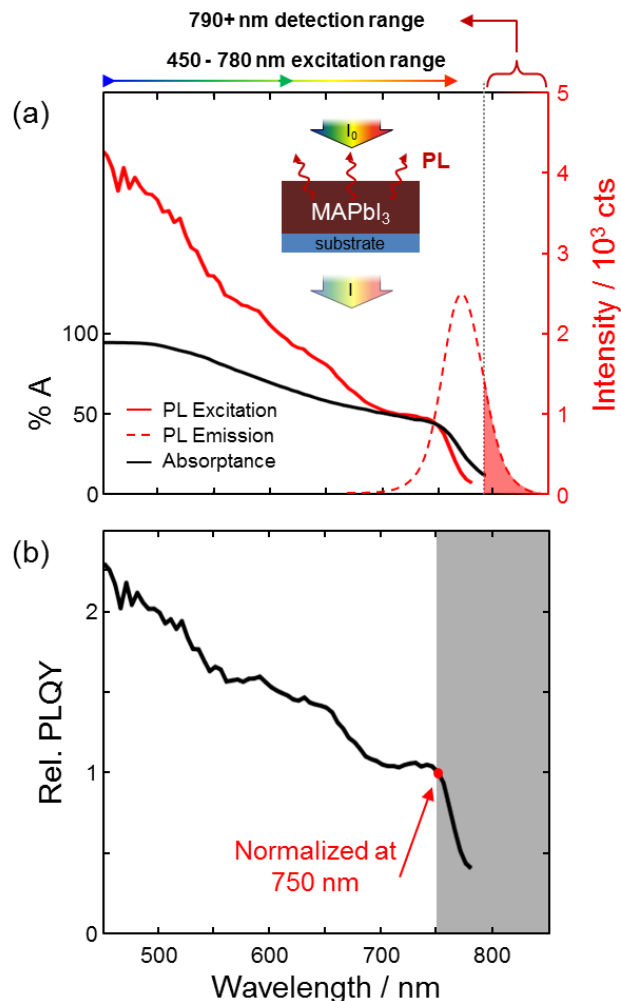

Figure 1. (a) Absorptance (%A, black trace), PLE (red/solid trace) and PL emission (red/dashed trace) spectra. The red shaded region indicates which part of the PL emission band is integrated for the PLE signal. Inset schematic demonstrates the measurement geometry where PL is detected in the same direction of the incoming light and $\%A = (1-I/I_0) \times 100$. (b) Relative PLQY spectrum acquired by dividing the PLE spectrum by the absorptance spectrum. The PLQY

spectrum is normalized at 750 nm. The grey shaded region indicates the spectral range (>750 nm) where uncertainty is high due to a low PLE signal.

Figure 1a shows the PLE and the absorptance (%A) spectra of an MAPbI$_3$ film prior to extensive light-soaking. We can quantify the difference by extracting the relative PL quantum yield spectrum (henceforth just PLQY), which we acquire by dividing the PLE spectrum by the absorptance spectrum (Figure 1b), and observe the yield is twice as high at 450 nm compared to 750 nm. We have indications that this may be related to the amount of excess/lack of PbI$_2$ formed in the perovskite, which is obtained by varying the PbI$_2$/MAI precursor molar ratios (see Figure S4), although more extensive measurements are required to verify this with better certainty.

The Spectral Fingerprint of PbI$_2$

We performed simultaneous PLE/absorptance measurements for 120 consecutive excitation scans, extracting PLQY spectra in each round. We measured in ambient air with a relative humidity around 40%, which are conditions typical for PbI$_2$ formation under light exposure[8] (see Figure S5 for measurements in dry nitrogen). The 2D maps in Figures 2a,b show the evolution of the absorptance and normalized PLQY spectra during the 6 hour measurement, with selected spectra from three instances plotted in Figures 2c,d. From the absorptance we verify that MAPbI$_3$ decomposes into PbI$_2$. After 2.5 hours, we find that the PLQY starts to drop off for a very distinct spectral range (between 450 nm – 520 nm), forming what we will refer to as a "dip" in the PLQY spectrum which coincides with the absorption of PbI$_2$. We explain this as photons that

are absorbed in PbI_2 and generate charge carriers are parasitically lost (filter effect),[39] even if they recombine radiatively since PbI_2 emission (~520 nm) is filtered out in our detection scheme (see Figure 1a).

Figure 2b shows that the normalized PLQY spectrum remains unchanged for the first few hours, although the non-normalized spectra (Figure S6) demonstrate that there is a significant PL enhancement prior to any degradation. The general consensus in the community is that an increase in the PLQY during light-soaking is related to passivation/annihilation of defects, although it is still debated whether this is mediated by atmospheric species (O_2, H_2O),[40–42] migrating ions,[43] and/or PbI_2 itself.[16] Quitsch and co-workers recently demonstrated a strong dependence of photo-induced PL enhancement/degradation on excitation wavelength, where enhancement (photo-brightening) was exclusively reported for excitation wavelengths longer than 520 nm.[44] Since we here focus on the photo-induced formation of PbI_2 (degradation), normalizing the PLQY spectra at 750 nm removes the spectral signature of photo-brightening (observed for longer wavelengths), which isolates the signature of PbI_2 formation as shown in Figure 2d.
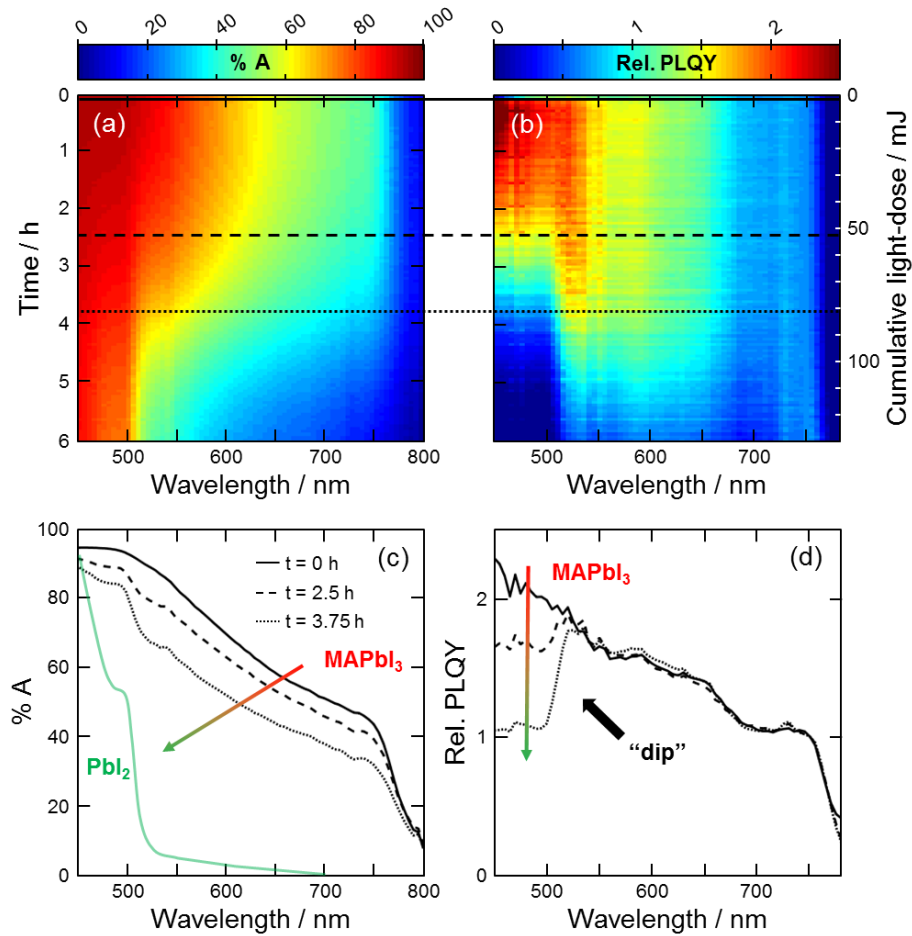
Figure 2. 2D maps showing the temporal evolution of (a) absorptance and (b) normalized PLQY spectra during 6 hours of light-soaking. PLQY spectra are normalized at 750 nm. The right vertical axis shows the cumulative light-dose throughout the experiment. (c,d) Selected spectra from the two maps at three points in time, t = 0 h (solid), t = 2.5 h (dashed) and t = 3.75 h (dotted). The PbI$_2$ absorption spectrum in (c) is adapted with permission from[45]. The "dip" in (d) is the indicator of PbI$_2$ formation.

Spectrally & Temporally Resolved PL

We acquire PLQY spectra (Figure 3a) with intermittent measurements of the PL decay kinetics using 450 nm and 700 nm excitation wavelengths (Figure 3b) during 600 min of light-soaking. We employ the time-correlated single photon counting (TCSPC) method and fit the PL decays with a stretched exponential function from which we extract the average lifetimes (Figure 3c) as detailed in SI Note 2 (measurement) and SI Note 3 (fitting). Prior to any extensive light-soaking, the extracted lifetimes are similar for both excitation wavelengths. The mono-exponential nature of the decays points to the dominant recombination mechanism being trap-assisted,[46] which is consistent with the estimated photo-generated carrier density ($\Delta n \approx 10^{15}$ cm^{-3}, see SI note 2) being an order of magnitude lower than the trap density ($N_t \approx 10^{16}$ cm^{-3}) that is typically reported for solution processed MAPbI$_3$ films.[43,47] Even if the photon flux is kept constant, the carrier generation toward the excited surface (where we also detect PL) is expected to be slightly higher for 450 nm excitation since the absorption coefficient is higher, which is reflected in the marginally higher initial amplitude of the decay. However, we establish that at t = 0 min this difference in generation is not sufficient to induce a different recombination mechanism.

During the first few hours, the lifetimes of both decays increase in a similar fashion and maintain their mono-exponential shape while the PLQY also increases, which are both commonly reported signatures of photo-induced defect passivation[40] (see Figure S7 for non-normalized PLQY spectra). However, once the PbI$_2$ related dip emerges in the PLQY spectrum (t = 420 min), an additional fast component in the PL decay evolves only for 450 nm excitation. With further light soaking, the PbI$_2$-related PLQY dip increases while the discrepancy between the two PL decays becomes even more pronounced, which is demonstrated in Figure 3c.
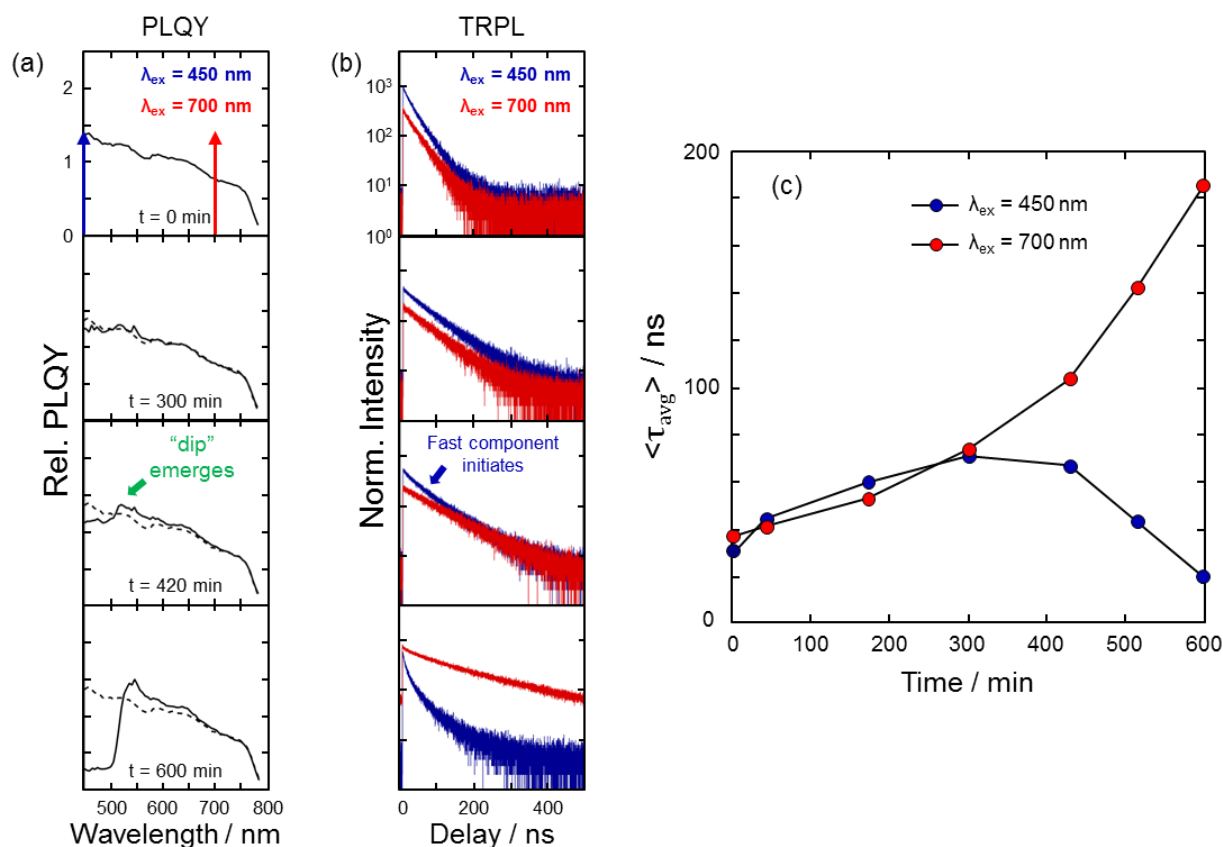
Figure 3. (a) PLQY spectra at four instances throughout the 10 hour light-soaking experiment. The dashed traces in the bottom three panels represent the PLQY at t = 0 min. Vertical scale is the same for all panels. (b) PL decays generated with 450 nm (blue traces) and 700 nm (red traces) excitation energies at the same time instances shown in (a). Vertical scale is the same for all panels. The two excitation wavelengths generating the PL decays in (b) are indicated by blue (450 nm) and red (700 nm) arrows in the top panel of (a). (c) Average lifetimes extracted using stretched exponential fits for both excitation wavelengths (see Figure S8 for the complete data set and fit parameters).

In Figure 3b we can see two distinct features in the PL kinetics evolve: (i) increasing of the slow decay component, which is observed as soon as light-soaking initiates, and (ii) increasing of

the fast decay component which has an onset after a few hours. Process (i) occurs for both excitation wavelengths, while process (ii) exclusively occurs for 450 nm. Regardless of the underpinning mechanism, we conclude that (i) appears as a result of passivation of non-radiative recombination channels as previously reported.[40] Process (ii) appears when a substantial dip in the PLQY spectrum (t = 420 min) emerges which, interestingly, only seems to be present when exciting in the spectral range of PbI_2 absorption (450 nm – 520 nm). As the detection excludes emission from PbI_2, we conclude that the carrier recombination kinetics can be altered in the perovskite by the mere presence of PbI_2, as long as photons are absorbed by it.

Probing the Recombination Mechanism

  Having indications of a different recombination mechanism in the perovskite that is active only when charge-carriers are generated in PbI_2, we investigate the effect of a 130 nm thick PbI_2 layer evaporated on top of a 400 nm thick $MAPbI_3$ thin film (see cross-section SEM in Figure 4a) and compare the PL kinetics to a reference sample without any evaporated PbI_2. Assuming similar absorption coefficients for PbI_2 and $MAPbI_3$,[48] the 130 nm PbI_2 layer should absorb approx. 75-80 % of photons for excitation wavelengths between 450 nm – 520 nm. The non-normalized PLQY spectrum in comparison to the reference sample (without a PbI_2 layer) not only verifies that the so-called "dip" is related to PbI_2, but also shows that there is a two-fold increase of the PLQY for wavelengths longer than 520 nm (Figure 4b). This observation supports the notion that PbI_2 passivates the $MAPbI_3$ surface,[16,30] although our results suggests it is only visible when probed with excitation wavelengths longer than 520 nm.

The PLQY of the sample containing a layer of PbI_2 is approx. 80% lower in the range of the dip compared to the reference sample, which is similar to the percentage of expected photon-absorption in PbI_2. From the PLQY alone, it would therefore seem that the detected emission comes from charge carriers that are directly generated in $MAPbI_3$ via absorption of photons that manage to penetrate through the PbI_2 layer (for λ_{ex} = 450 nm - 520 nm). However, when comparing the PL decays at 450 nm and 700 nm we see the same discrepancy as previously observed (Figure 4c). We cannot rationalize why such different PL kinetics are observed between the two excitation wavelengths with only a marginal difference in the charge carrier concentration directly generated in $MAPbI_3$ (depth-resolved carrier generation profiles schematically drawn in Figure 4a are estimated from α in ref. 48). Furthermore, such a scenario would require a 100% radiative yield of the carriers generated in the $MAPbI_3$ layer for 450 nm excitation in order to explain the matching PLQY reduction and estimated parasitic losses, which finds no support in literature for the films investigated here. We therefore conclude there must be a radiative component that is missing in our analysis.

We measure PL decays at various pulse fluences with the two excitation wavelengths (450 nm and 700 nm). When exciting through the PbI_2 layer first, it becomes evident that there is a carrier density dependent recombination mechanism present only for 450 nm excitation (Figure 4d – λ_{ex} = 450 nm, Figure 4e – λ_{ex} = 700 nm). Measuring through the substrate side of the sample, thus absorbing directly into $MAPbI_3$, both excitation wavelengths generate similar monoexponential PL decays (Figure S8). We therefore relate the emerging fast component to a higher order bimolecular recombination process which is enabled by the presence of PbI_2.

The pulse fluences where bimolecular recombination becomes dominant are relatively low (a few nJ/cm^2) compared to other reports on similarly prepared perovskite thin films.[47]

Furthermore, we demonstrated in the light-soaking experiment (Figure 3) that the PL decay changes without altering the pulse fluence. This suggests that the predominant recombination mechanism transitions from monomolecular to bimolecular recombination with the formation of PbI_2 alone. Indeed, we have indications that photo-induced passivation of defects is at play (photo-brightening), but if N_t were to reduce to a point where bimolecular recombination becomes relevant ($\Delta n \approx N_t$), we should see this expressed in the PL decays generated with all excitation wavelengths. Since this is not the case (see Figure S8), we find the most logical explanation to be that the actual volume into which charge carriers accumulate and recombine is much smaller than previously estimated for the entire film with thickness d = 400 nm. This consequently yields an effective carrier density (Δn_e) that could be orders of magnitude larger than Δn. Therefore, if charge carriers become confined by some mechanism induced by PbI_2, bimolecular recombination could indeed become the predominant recombination mechanism even with a rather low incident flux.
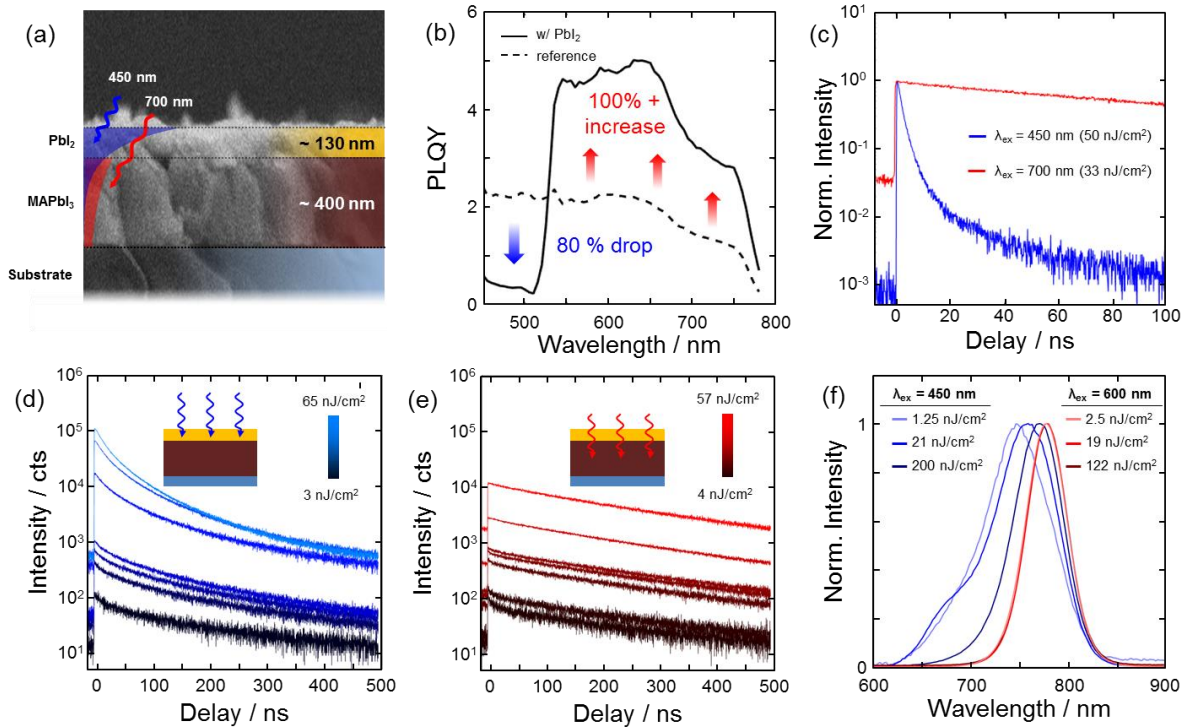
Figure 4. (a) Cross-section SEM showing the thickness of the evaporated PbI_2 layer (~130 nm) as well as the $MAPbI_3$ layer (~400 nm). Blue and red shaded regions show the carrier generation profiles with 450 nm and 700 nm excitation wavelengths respectively when exciting with the same photon flux. (b) PLQY of the PbI_2 - evaporated sample (solid) in comparison to a reference film without a PbI_2 layer (dashed). The blue arrow indicates the "dip" (reduction of PLQY) due to PbI_2 and the red arrow indicates the subsequent two-fold PL enhancement. (c) PL decays acquired for λ_{ex} = 450 nm (blue) and λ_{ex} = 700 nm (red). (d,e) Fluence dependent PL decay curves for 450 nm (black/blue traces) and for 700 nm (black/red traces). The schematics show from which direction the sample is excited, where PL is collected from the same side. (f) Fluence dependent PL spectra acquired with 450 nm excitation (blue traces) and 600 nm excitation (red traces) with long-pass emission filter at 610 nm.

We measure the PL spectra with 450 nm excitation as a function of excitation density (exciting through the PbI_2 layer) with a long-pass filter at 610 nm. At the lowest fluence, we observe that there is a strong blue-shift and broadening of the PL band. In fact, rather than a single emission band, the irregular shape of the blue-shifted PL spectra is indicative of a collection of overlapping bands. With higher fluence, the PL spectrum red-shifts and becomes more narrow. With $\lambda_{ex} = 600$ nm we excite $MAPbI_3$ directly and not via PbI_2, and the PL emission peak remains at 775 nm and exhibits no shift or broadening/narrowing when changing excitation density (Figure 4f). Measuring through the substrate side first (direct absorption by $MAPbI_3$) we see a steady, non-shifting nor broadening PL spectrum centered at 775 nm (Figure S9) for both excitation wavelengths. We therefore conclude that the blue-shifted emission is caused by direct excitation into PbI_2 and consequently relate the blue-shifted emission to the PbI_2-enabled bimolecular recombination.

We acquire PL images generated with excitation wavelengths ranging from 450 nm to 600 nm (see SI Note 2 for details). Figure 5a shows two PL images of the same region generated with 450 nm and 700 nm where bright domains are observed only for the former. These domains disappear once the excitation wavelength is longer than 520 nm (see Figures S10-11 for PL images with excitation wavlengths between 450 nm – 600 nm). This points to the PL emission related to the PbI_2-enabled recombination mechanism coming from localized domains, which also supports the notion that the recombination mechanism is induced by charge carriers becoming confined when generated in PbI_2.
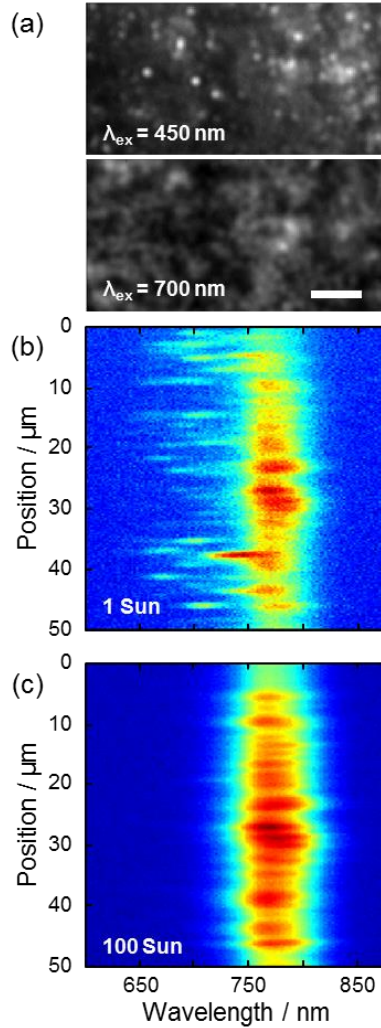
Figure 5. (a) PL images of the same region measured with λ_{ex} = 450 nm (top) and λ_{ex} = 700 nm (bottom) showing bright emissive domains with the former. The scale bar represents 5 μm. (b) Spatially resolved PL spectra identifying a distribution of blue-shifted PL peaks related to the emissive domains observed in (a) for an excitation density of 1 Sun. (c) Spatially resolved spectra from same region with excitation density increased to 100 Sun where the blue-shifted peaks disappear. Excitation wavelength in (b) and (c) is 450 nm.

We also extract spatially resolved spectra from a ~2 μm wide vertical segment of the image and capture the PL spectra of these bright domains when exciting with 450 nm. Each horizontal line in Figures 5b-c represent the spectrum from a point in the vertical segment from the image (see SI Note 2 for details). It becomes evident that not only do the bright domains exhibit blue-shifted emission, but also that there is a distribution of how large the shift is (Figure 5b), which explains the irregular shape of the spatially averaged PL spectra in Figure 4f. Moreover, as the fluence is increased by two orders of magnitude, the blue-shifted localized emission disappears, showing only the expected emission from $MAPbI_3$ at 775 nm (Figure 5c).

$PbI_2/MAPbI_3$ Interface Assisted Recombination

Since we observe a red-shift of the emission toward that of pristine $MAPbI_3$ with increasing power (Figure 5c), we rule out the Burstein-Moss effect (band-filling)[49] as the mechanism giving rise to the spectral shifts. We previously reported blue-shifted PL in $MAPbI_3$ single crystals and films arising from intermediate phases between the $MAPbI_3$ and PbI_2 structure exhibiting distortions and difference in connectivity between lead-halide octahedra due to the loss of structure-stabilizing methylammonium cations.[11,50] This spatial gradient of lattice distortion consequently gives rise to a bandgap gradient, increasing in energy from $MAPbI_3$ towards PbI_2 regions. We therefore propose that as PbI_2 forms in the perovskite, whether via a photo-induced process or evaporation, it gives rise to a transition phase at the $PbI_2/MAPbI_3$ interface comprising a small volume which alters the recombination kinetics. Our observations suggest that the Δn_e giving rise to the higher order recombination mechanism arises due to the confinement of charge

carriers, from which we find it likely that charge carriers generated in PbI_2 funnel into the relatively small volume of the disordered interface.

Supasai and co-workers demonstrated quite early that PbI_2 induces defect-formation at the interface to $MAPbI_3$, which could certainly trap charge carriers funnelled from PbI_2.[15] Once trapped, carriers may recombine and yield emission with higher energy than the $MAPbI_3$ bandgap. It is also reported that carrier mobility is reduced in a disordered energy landscape which also, according to Langevin theory, should increase the rate of free electron/hole recombination.[51] Regardless of the mechanism via which charge-carriers accumulate, we conclude that radiative recombination must occur with a transition energy higher than the $MAPbI_3$ bandgap. Figure 5b shows that a low fluence yields a broad emission which arises from both the PbI_2/$MAPbI_3$ interface and bulk $MAPbI_3$. As fluence increases, the interface saturates due to its relatively small volume which leads to more carriers transferring to the $MAPbI_3$ bulk where emission at 775 nm becomes dominant. Therefore, increasing the fluence high enough manifests as a red-shift and narrowing of the PL emission.

Direct absorption into the transition phase with excitation wavelengths longer than 520 nm should also occur, but since this phase comprises such a small volume in the film, the majority of photons are absorbed in the $MAPbI_3$ bulk yielding emission at 775 nm, with the predominant recombination mechanism being monomolecular (judging from the decays in Figures 3 and 4 for $\lambda_{ex} > 520$ nm). Thus, population of the transition phase with charge carriers is most effective when injecting them via PbI_2. We summarize the proposed recombination mechanism occurring at the PbI_2/$MAPbI_3$ interface in Figure 6.
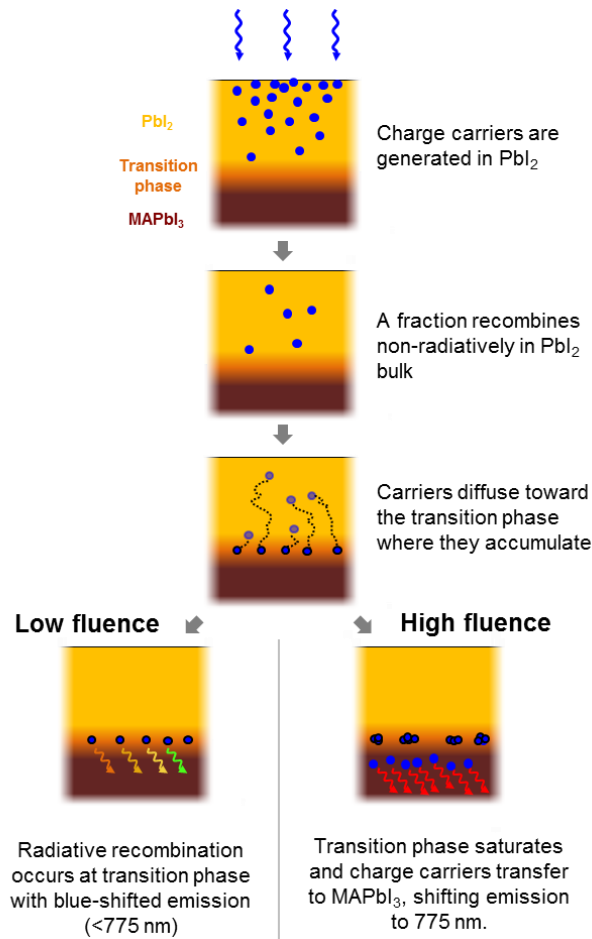
Figure 6. Schematic demonstrating the recombination mechanism via PbI$_2$ with an excitation wavelength within the range of PbI$_2$ absorption (450 nm – 520 nm) at low *vs.* high fluence. Charge carriers are first generated by direct absorption in PbI$_2$ (top) after which a fraction recombines non-radiatively in the PbI$_2$ bulk. Remaining charge-carriers diffuse to the transition phase where they accumulate and effectively yield a high carrier density. This subsequently leads to an increased rate of radiative recombination having blue shifted PL emission. As fluence increases, the transition phase saturates and recombination in the MAPbI$_3$ bulk becomes successively more dominant causing the PL emission to shift toward 775 nm, while also becoming narrower.

In summary, we have presented an in-depth spectroscopic study on the role of PbI_2 in $MAPbI_3$ thin films when it has been formed as a photo-induced degradation product, and via vapour-assisted deposition. Combining measurements of PLQY and TRPL we identify three optical signatures that can be used to detect the presence of PbI_2 in $MAPbI_3$ thin films: (i) parasitic absorption, (ii) a fast recombination component in the PL decay, and (iii) a blue-shift of PL emission. Each of these phenomena exhibits a dependence on excitation wavelength and the geometry in which the sample is excited when PbI_2 is present. Furthermore, these signatures are only present when charge carriers are generated in PbI_2 directly. Thus, depending on the configuration in which the measurement is made, one can acquire some information in regard to where in the perovskite bulk the predominant presence of PbI_2 is (i.e. toward the top or the bottom surface of the film).

We also characterize the underpinning mechanism giving rise to phenomena (ii) and (iii) as a radiative bimolecular recombination mechanism occurring in a confined volume at the $PbI_2/MAPbI_3$ interface. Since charge-carriers accumulate in a small volume, bimolecular recombination may still occur despite a relatively low incident photon flux. Thus, as PbI_2 induces parasitic losses for photons in the range between 450 nm – 520 nm, our results imply that a relevant portion of these charge carriers may in fact contribute to the open-circuit voltage of the perovskite. We therefore provide insight to the open debate regarding the beneficial/detrimental aspect of excess PbI_2 amount with a simple picture where we assume that the interface between PbI_2 and $MAPbI_3$ contributes to the beneficial aspect (radiative recombination) and the bulk PbI_2 contributes to the detrimental aspect (non-radiative recombination). Thus, the surface-to-volume ratio of PbI_2 domains within the perovskite bulk, and also where in relation to the incoming light they form, may largely affect the overall recombination kinetics. Finally, the notion of PbI_2

acting as a funnel for charge-carriers to a defined region in space could certainly inspire new designs for device applications, not only for perovskite photovoltaics, but for material science in general.

Supporting Information

Sample preparation with XRD and SEM characterization, experimental setup and measurement procedures, stretched exponential fitting, measurements on precursor modified $MAPbI_3$, measurements in N_2 vs. air, PLQY data without normalization, TRPL of all excitation wavelengths and analysis, fluence dependent TRPL and PL spectra, PL images with different excitation wavelengths.

Corresponding Authors:

aboma.merdasa@helmholtz-berlin.de,
eva.unger@helmholtz-berlin.de
ivan.scheblykin@chemphys.lu.se

Orcid ID

Aboma Merdasa: 0000-0002-6298-5672
Mojtaba Abdi-Jalebi: 0000-0002-9430-6371
Boris Louis: 0000-0003-2882-6907
Marina Gerhard: 0000-0002-6539-4675
Samuel D. Stranks: 0000-0002-8303-7292
Eva L. Unger: 0000-0002-3343-867X
Ivan G. Scheblykin: 0000-0001-6059-4777

Notes

Acknowledgements

References

(1) Kojima, A.; Teshima, K.; Shirai, Y.; Miyasaka, T. Organometal Halide Perovskites as Visible-Light Sensitizers for Photovoltaic Cells. *J. Am. Chem. Soc.* **2009**, *131* (17), 6050–6051.

(2) Lee, M. M.; Teuscher, J.; Miyasaka, T.; Murakami, T. N.; Snaith, H. J. Efficient Hybrid Solar Cells Based on Meso-Superstructured Organometal Halide Perovskites. *Science* **2012**, *338* (6107), 643–647.

(3) Jeon, N. J.; Na, H.; Jung, E. H.; Yang, T. Y.; Lee, Y. G.; Kim, G.; Shin, H. W.; Il Seok,

S.; Lee, J.; Seo, J. A Fluorene-Terminated Hole-Transporting Material for Highly Efficient and Stable Perovskite Solar Cells. *Nat. Energy* **2018**, *3* (August), 682–689.

(4)   Abdi-Jalebi, M.; Andaji-Garmaroudi, Z.; Cacovich, S.; Stavrakas, C.; Philippe, B.; Richter, J. M.; Alsari, M.; Booker, E. P.; Hutter, E. M.; Pearson, A. J.; et al. Maximizing and Stabilizing Luminescence from Halide Perovskites with Potassium Passivation. *Nature* **2018**, *555* (7697), 497–501.

(5)   Sanchez, S.; Christoph, N.; Grobety, B.; Phung, N.; Steiner, U.; Saliba, M.; Abate, A. Efficient and Stable Inorganic Perovskite Solar Cells Manufactured by Pulsed Flash Infrared Annealing. *Adv. Energy Mater.* **2018**, 1802060.

(6)   Wang, Z.; Lin, Q.; Wenger, B.; Christoforo, M. G.; Lin, Y. H.; Klug, M. T.; Johnston, M. B.; Herz, L. M.; Snaith, H. J. High Irradiance Performance of Metal Halide Perovskites for Concentrator Photovoltaics. *Nat. Energy* **2018**, *3* (October), 1013.

(7)   Misra, R. K.; Aharon, S.; Li, B.; Mogilyansky, D.; Visoly-Fisher, I.; Etgar, L.; Katz, E. a. Temperature- and Component-Dependent Degradation of Perovskite Photovoltaic Materials under Concentrated Sunlight. *J. Phys. Chem. Lett.* **2015**, *6*, 326–330.

(8)   Yang, J.; Siempelkamp, B. D.; Liu, D.; Kelly, T. L. Investigation of $CH_3NH_3PbI_3$ degradation Rates and Mechanisms in Controlled Humidity Environments Using in Situ Techniques. *ACS Nano* **2015**, *9* (2), 1955–1963.

(9)   Niu, G.; Li, W.; Meng, F.; Wang, L.; Dong, H.; Qiu, Y. Study on the Stability of $CH_3NH_3PbI_3$ Films and the Effect of Post-Modification by Aluminum Oxide in All-Solid-State Hybrid Solar Cells. *J. Mater. Chem. A* **2014**, *2* (3), 705–710.

(10)   Nickel, N. H.; Lang, F.; Brus, V. V.; Shargaieva, O.; Rappich, J. Unraveling the Light-Induced Degradation Mechanisms of $CH_3NH_3PbI_3$ Perovskite Films. *Adv. Electron. Mater.* **2017**, 1700158.

(11)   Merdasa, A.; Bag, M.; Tian, Y.; Källman, E.; Dobrovolsky, A.; Scheblykin, I. G. Super-Resolution Luminescence Micro-Spectroscopy Reveals Mechanism of Photo-Induced Degradation in $CH_3NH_3PbI_3$ Perovskite Nano-Crystals. *J. Phys. Chem. C* **2016**, *120*, 10711−10719.

(12)   Khenkin, M. V.; K. M., A.; Visoly-Fisher, I.; Kolusheva, S.; Galagan, Y.; Di Giacomo, F.; Vukovic, O.; Patil, B. R.; Sherafatipour, G.; Turkovic, V.; et al. Dynamics of Photoinduced Degradation of Perovskite Photovoltaics: From Reversible to Irreversible Processes. *ACS Appl. Energy Mater.* **2018**, *1*, 799–806.

(13)   Yuan, H.; Debroye, E.; Janssen, K.; Naiki, H.; Steuwe, C.; Lu, G.; Moris, M.; Orgiu, E.; Uji-I, H.; De Schryver, F.; et al. Degradation of Methylammonium Lead Iodide Perovskite Structures through Light and Electron Beam Driven Ion Migration. *J. Phys. Chem. Lett.* **2016**, *7* (3), 561−566.

(14)   Motoki, K.; Miyazawa, Y.; Kobayashi, D.; Ikegami, M.; Miyasaka, T.; Yamamoto, T.; Hirose, K. Degradation of $CH_3NH_3PbI_3$ perovskite Due to Soft X-Ray Irradiation as Analyzed by an X-Ray Photoelectron Spectroscopy Time-Dependent Measurement Method. *J. Appl. Phys.* **2017**, *121* (8), 1–5.

(15)   Supasai, T.; Rujisamphan, N.; Ullrich, K.; Chemseddine, A.; Dittrich, T. Formation of a Passivating $CH_3NH_3PbI_3$ / PbI_2 Interface during Moderate Heating of $CH_3NH_3PbI_3$

Layers. *Appl. Phys. Lett.* **2013**, *103*, 183906.

(16)   Chen, Q.; Zhou, H.; Song, T. Bin; Luo, S.; Hong, Z.; Duan, H. S.; Dou, L.; Liu, Y.; Yang, Y. Controllable Self-Induced Passivation of Hybrid Lead Iodide Perovskites toward High Performance Solar Cells. *Nano Lett.* **2014**, *14* (7), 4158–4163.

(17)   Cao, D. H.; Stoumpos, C. C.; Malliakas, C. D.; Katz, M. J.; Farha, O. K.; Hupp, J. T.; Kanatzidis, M. G. Remnant PbI2, an Unforeseen Necessity in High-Efficiency Hybrid Perovskite-Based Solar Cells? *APL Mater.* **2014**, *2* (9), 091101.

(18)   Somsongkul, V.; Lang, F.; Jeong, A. R.; Rusu, M.; Arunchaiya, M.; Dittrich, T. Hole Blocking $PbI_2/CH_3NH_3PbI_3$ Interface. *Phys. Status Solidi - Rapid Res. Lett.* **2014**, *8* (9), 763–766.

(19)   Calloni, A.; Abate, A.; Bussetti, G.; Berti, G.; Yivlialin, R.; Ciccacci, F.; Duò, L. Stability of Organic Cations in Solution-Processed $CH_3NH_3PbI_3$ Perovskites: Formation of Modified Surface Layers. *J. Phys. Chem. C* **2015**, *119* (37), 21329–21335.

(20)   Park, B. wook; Kedem, N.; Kulbak, M.; Lee, D. Y.; Yang, W. S.; Jeon, N. J.; Seo, J.; Kim, G.; Kim, K. J.; Shin, T. J.; et al. Understanding How Excess Lead Iodide Precursor Improves Halide Perovskite Solar Cell Performance. *Nat. Commun.* **2018**, *9* (1), 1–8.

(21)   Kim, Y. C.; Jeon, N. J.; Noh, J. H.; Yang, W. S.; Seo, J.; Yun, J. S.; Ho-baillie, A.; Huang, S.; Green, M. A.; Seidel, J.; et al. Beneficial Effects of PbI_2 Incorporated in Organo-Lead Halide Perovskite Solar Cells. *Adv. Energy Mater.* **2016**, *6*, 1502104.

(22)   Roldán-Carmona, C.; Gratia, P.; Zimmermann, I.; Grancini, G.; Gao, P.; Graetzel, M.;

Nazeeruddin, M. K. High Efficiency Methylammonium Lead Triiodide Perovskite Solar Cells: The Relevance of Non-Stoichiometric Precursors. *Energy Environ. Sci.* **2015**, *8* (12), 3550–3556.

(23) Lee, Y. H.; Luo, J.; Humphry-Baker, R.; Gao, P.; Grätzel, M.; Nazeeruddin, M. K. Unraveling the Reasons for Efficiency Loss in Perovskite Solar Cells. *Adv. Funct. Mater.* **2015**, *25* (25), 3925–3933.

(24) Jacobsson, T. J.; Correa-Baena, J. P.; Halvani Anaraki, E.; Philippe, B.; Stranks, S. D.; Bouduban, M. E. F.; Tress, W.; Schenk, K.; Teuscher, J.; Moser, J. E.; et al. Unreacted PbI$_2$ as a Double-Edged Sword for Enhancing the Performance of Perovskite Solar Cells. *J. Am. Chem. Soc.* **2016**, *138* (32), 10331–10343.

(25) Hsu, H. Y.; Ji, L.; Du, M.; Zhao, J.; Yu, E. T.; Bard, A. J. Optimization of PbI$_2$/MAPbI$_3$ Perovskite Composites by Scanning Electrochemical Microscopy. *J. Phys. Chem. C* **2016**, *120* (35), 19890–19895.

(26) Gujar, T. P.; Unger, T.; Schönleber, A.; Fried, M.; Panzer, F.; van Smaalen, S.; Köhler, A.; Thelakkat, M. The Role of PbI$_2$ on CH$_3$NH$_3$PbI$_3$ Perovskite Stability, Solar Cell Parameters and Device Degradation. *Phys. Chem. Chem. Phys.* **2017**, *85*, 605–614.

(27) Adhikari, N.; Dubey, A.; Khatiwada, D.; Mitul, A. F.; Wang, Q.; Venkatesan, S.; Iefanova, A.; Zai, J.; Qian, X.; Kumar, M.; et al. Interfacial Study to Suppress Charge Carrier Recombination for High Efficiency Perovskite Solar Cells. *ACS Appl. Mater. Interfaces* **2015**, *7* (48), 26445–26454.

(28) Wang, S.; Dong, W.; Fang, X.; Zhang, Q.; Zhou, S.; Deng, Z.; Tao, R.; Shao, J.; Xia, R.;

Song, C.; et al. Credible Evidence for the Passivation Effect of Remnant PbI_2 in $CH_3NH_3PbI_3$ Films in Improving the Performance of Perovskite Solar Cells. *Nanoscale* **2016**, *8* (12), 6600–6608.

(29)   Ma, Y.; Vashishtha, P.; Chen, K.; Peach, E. L.; Ohayon, D.; Hodgkiss, J. M.; Halpert, J. E. Controlled Growth of $CH_3NH_3PbI_3$ Using a Dynamically Dispensed Spin-Coating Method: Improving Efficiency with a Reproducible PbI_2 Blocking Layer. *ChemSusChem* **2017**, *10* (12), 2677–2684.

(30)   Kheraj, V.; Simonds, B. J.; Toshniwal, A.; Misra, S.; Peroncik, P.; Zhang, C.; Vardeny, Z. V; Scarpulla, M. A. Using Photoluminescence to Monitor the Optoelectronic Properties of Methylammonium Lead Halide Perovskites in Light and Dark over Periods of Days. *J. Lumin.* **2018**, *194* (October 2017), 353–358.

(31)   Chen, S.; Wen, X.; Yun, J. S.; Huang, S.; Green, M.; Jeon, N. J.; Yang, W. S.; Noh, J. H.; Seo, J.; Seok, S. Il; et al. Spatial Distribution of Lead Iodide and Local Passivation on Organo-Lead Halide Perovskite. *ACS Appl. Mater. Interfaces* **2017**, *9* (7), 6072–6078.

(32)   Wang, H.; Hao, M.; Han, J.; Yu, M.; Qin, Y.; Zhang, P.; Guo, Z.; Ai, X.-C.; Zhang, J.-P. The Adverse Effects of Excessively Remained PbI_2 on Photovoltaic Performance , Charge Separation and Trap State Properties in Mesoporous Structured Perovskite Solar Cells. *Chem. Eur. J.* **2017**, *23*, 3986–3992.

(33)   Kirchartz, T.; Krückemeier, L.; Unger, E. L. Research Update: Recombination and Open-Circuit Voltage in Lead-Halide Perovskites. *APL Mater.* **2018**, *6* (10), 100702.

(34)   Stolterfoht, M.; Wolff, C. M.; Márquez, J. A.; Zhang, S.; Hages, C. J.; Rothhardt, D.;

Albrecht, S.; Burn, P. L.; Meredith, P.; Unold, T.; et al. Visualization and Suppression of Interfacial Recombination for High-Efficiency Large-Area Pin Perovskite Solar Cells. *Nat. Energy* **2018**, *3* (October), 847–854.

(35) Tress, W.; Marinova, N.; Inganäs, O.; Nazeeruddin, M. K.; Zakeeruddin, S. M.; Graetzel, M. Predicting the Open-Circuit Voltage of $CH_3NH_3PbI_3$ Perovskite Solar Cells Using Electroluminescence and Photovoltaic Quantum Efficiency Spectra : The Role of Radiative and Non-Radiative Recombination. *Adv. Energy Mater.* **2015**, *5*, 1400812.

(36) Kirchartz, T.; Rau, U. What Makes a Good Solar Cell? *Adv. Energy Mater.* **2018**, *8*, 1703385.

(37) Stranks, S. D.; Burlakov, V. M.; Leijtens, T.; Ball, J. M.; Goriely, A.; Snaith, H. J. Recombination Kinetics in Organic-Inorganic Perovskites: Excitons, Free Charge, and Subgap States. *Phys. Rev. Appl.* **2014**, *2* (3), 1–8.

(38) Stranks, S. D.; Petrozza, A. Revisiting Photocarrier Lifetimes in Photovoltaics. *Nat. Publ. Gr.* **2016**, *10* (9), 562.

(39) Melvin, A. A.; Stoichkov, V. D.; Kettle, J.; Mogilyansky, D.; Katz, E. A.; Visoly-Fisher, I. Lead Iodide as a Buffer Layer in UV-Induced Degradation of $CH_3NH_3PbI_3$ films. *Sol. Energy* **2018**, *159*, 794–799.

(40) Tian, Y.; Peter, M.; Unger, E.; Abdellah, M.; Zheng, K.; Pullerits, T.; Yartsev, A.; Sundström, V.; Scheblykin, I. G. Mechanistic Insights into Perovskite Photoluminescence Enhancement: Light Curing with Oxygen Can Boost Yield Thousandfold. *Phys. Chem. Chem. Phys.* **2015**, *17*, 24978–24987.

(41) Brenes, R.; Eames, C.; Bulović, V.; Islam, M. S.; Stranks, S. D. The Impact of Atmosphere on the Local Luminescence Properties of Metal Halide Perovskite Grains. *Adv. Mater.* **2018**, *30* (15), 1–8.

(42) Fang, H. H.; Wang, F.; Adjokatse, S.; Zhao, N.; Loi, M. A. Photoluminescence Enhancement in Formamidinium Lead Iodide Thin Films. *Adv. Funct. Mater.* **2016**, *26* (26), 4653–4659

(43) DeQuilettes, D. W.; Zhang, W.; Burlakov, V. M.; Graham, D. J.; Leijtens, T.; Osherov, A.; Snaith, H. J.; Ginger, D. S.; Stranks, S. D. Photo-Induced Halide Redistribution in Organic–inorganic Perovskite Films. *Nat. Commun.* **2016**, *7* (May), 11683.

(44) Quitsch, W.-A.; deQuilettes, D. W.; Pfingsten, O.; Schmitz, A.; Ognjanovic, S.; Jariwala, S.; Koch, S.; Winterer, M.; Ginger, D. S.; Bacher, G. The Role of Excitation Energy in Photobrightening and Photodegradation of Halide Perovskite Thin Films. *J. Phys. Chem. Lett.* **2018**, 2062–2069.

(45) Wu, Y.; Islam, A.; Yang, X.; Qin, C.; Liu, J.; Zhang, K.; Peng, W.; Han, L. Retarding the Crystallization of PbI2for Highly Reproducible Planar-Structured Perovskite Solar Cells via Sequential Deposition. *Energy Environ. Sci.* **2014**, *7* (9), 2934–2938.

(46) Herz, L. M. Charge-Carrier Dynamics in Organic-Inorganic Metal Halide Perovskites. *Annu. Rev. Phys. Chem.* **2016**, *67* (1), 65–89.

(47) Johnston, M. B.; Herz, L. M. Hybrid Perovskites for Photovoltaics: Charge-Carrier Recombination, Diffusion, and Radiative Efficiencies. *Acc. Chem. Res.* **2016**, *49* (1), 146–154.

(48)   Green, M. A.; Jiang, Y.; Soufiani, A. M.; Ho-Baillie, A. Optical Properties of Photovoltaic Organic-Inorganic Lead Halide Perovskites. *J. Phys. Chem. Lett.* **2015**, *6* (23), 4774–4785.

(49)   Manser, J. S.; Kamat, P. V. Band Filling with Free Charge Carriers in Organometal Halide Perovskites. *Nat. Photonics* **2014**, *8*, 737–743.

(50)   Filip, M. R.; Eperon, G. E.; Snaith, H. J.; Giustino, F. Steric Engineering of Metal-Halide Perovskites with Tunable Optical Band Gaps. *Nat. Commun.* **2014**, *5*, 5757.

(51)   Herz, L. M. Charge-Carrier Mobilities in Metal Halide Perovskites: Fundamental Mechanisms and Limits. *ACS Energy Lett.* **2017**, *2* (7), 1539–1548.